Performance of the correlated painting based on the mechanical structure of the anticorrelated painting scheme

Ming-Yang Huang,[1,2,3] Yoshiro Irie,[4] Shou-Yan Xu,[1,3] Xin Qi,[1,3] and Sheng Wang[1,2,3,*]

[1]*Institute of High Energy Physics, Chinese Academy of Sciences, Beijing 100049, China*
[2]*University of Chinese Academy of Sciences, Beijing 100049, China*
[3]*Spallation Neutron Source Science Center, Dongguan 523803, China*
[4]*High Energy Accelerator Research Organization (KEK), Tsukuba, Ibaraki 305-0801, Japan*

(Received 12 February 2022; accepted 7 November 2022; published 21 November 2022)

The China Spallation Neutron Source (CSNS) accelerator consists of an 80 MeV H^- Linac and a 1.6-GeV rapid cycling synchrotron (RCS). The painting scheme is one of the most important factors for the control of low beam loss at high beam power. In the painting injection of the CSNS/RCS, position scanning is used in both horizontal and vertical planes, and the anticorrelated painting is the design scheme. By using the anticorrelated painting, the beam power has successfully reached 50 kW. However, some problems have been found in the higher power beam commissioning, for instance, too large beam size after painting, nonuniform beam distribution, large transverse coupling effect, and so on, resulting in additional beam loss and making it difficult to satisfy the requirements of a high-power user mode. In order to solve these problems, flexibility in the CSNS design has been exploited to implement the correlated painting by using the rising current curve of the pulse power supply. The effectiveness of the new method has been verified in the simulation and beam commissioning, which can well control the full beam emittance and improve the beam distribution. By using the new method, the beam power on the target has successfully risen from 50 kW to the design value of 100 kW. Under the mechanical structure of the anticorrelated painting scheme where the position scanning is used in both horizontal and vertical planes, the correlated painting has been successfully achieved by using the rising current curve.

DOI: 10.1103/PhysRevAccelBeams.25.110401

I. INTRODUCTION

The China Spallation Neutron Source (CSNS) is a high power proton accelerator-based facility for the study of neutron scattering [1,2]. Its accelerator complex consists of an 80-MeV H^- Linac and a 1.6-GeV rapid cycling synchrotron (RCS) [3,4]. The RCS accumulates and accelerates an 80-MeV injection beam to 1.6 GeV and then extracts it to the target. The average beam power on the target is 100 kW, with a repetition rate of 25 Hz. Its lattice has a fourfold periodic structure with four long straight sections for the injection, extraction, rf cavity, and beam collimation, respectively.

The injection system in the CSNS/RCS [5,6] consists of four chicane bump magnets BC1–BC4, four horizontal painting magnets BH1–BH4, four vertical painting magnets BV1–BV4, two septum magnets (ISEP1 and ISEP2), a primary stripping foil (Str-1), and a secondary stripping foil (Str-2). Figure 1 shows the schematic diagram of the injection system.

Space-charge effects are the core problem of the high intensity proton accelerators [7–9]. In order to reduce the space-charge effects, the transverse phase space painting method [10–12] is used for injecting a small emittance beam from the Linac to the large ring acceptance. The transverse phase space painting method can be divided into correlated painting and anticorrelated painting. At present, the four spallation neutron sources in the world adopt

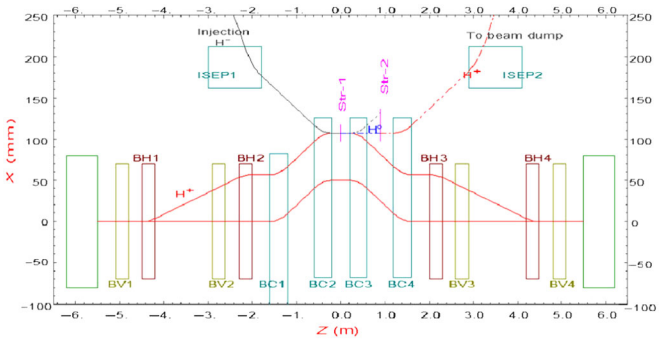

FIG. 1. The schematic diagram of the injection system.

*Corresponding author.
wangs@ihep.ac.cn

TABLE I. Related parameters of the space-charge forces for different machines.

	CSNS	J-PARC	SNS	ISIS
Injection beam energy (GeV)	0.08	0.4	1.0	0.08
Number of protons per pulse (10^{13})	1.56	8.3	15.0	2.8
Tune shift at the injection: $\Delta\nu$	0.28	0.15	0.15	0.4
Transition gamma: γ_t	4.9	9.2	5.2	5.1

different painting methods [13]. The anticorrelated painting is used for the Spallation Neutron Source at the Rutherford Appleton Laboratory (ISIS) [14,15]. The correlated painting is used for the Spallation Neutron Source at the Oak Ridge National Laboratory (SNS) [16,17]. The anticorrelated painting is the design scheme for the CSNS [5,18]. The Japan Accelerator Research Complex (J-PARC) [19–21] has the ability to switch between the correlated and anticorrelated painting because of the angular scanning in the vertical plane [22–26]. The correlated painting and anticorrelated painting are used, respectively, in different periods and different operating modes. Table I shows the related parameters of the space-charge forces for different machines [13]. It can be seen that the space-charge tune shift at the injection for the CSNS is larger than that of the J-PARC and SNS.

By using the anticorrelated painting, combined with other optimizations, the beam power of the CSNS accelerator has reached 50 kW and stable machine operation has been achieved [27]. However, in the higher power beam commissioning, a series of problems has been found with the anticorrelated painting, for instance, too large beam size after painting, nonuniform beam distribution, large transverse coupling effect, and so on, resulting in additional beam loss and making it difficult to satisfy the requirements of a stable high-power operation mode. In order to solve these problems, after detailed analysis, simulations, and experimental tests, flexibility in the CSNS design has been exploited to implement the correlated painting. The effectiveness of the correlated painting method has been verified in both simulation and beam commissioning. The correlated painting method is applied to the beam commissioning of the CSNS, which can well control the full beam emittance and improve the beam distribution.

The paper is organized as follows: In Sec. II, a comparative study between the anticorrelated and correlated painting is discussed and the advantages of the correlated painting method under the current injection scheme are presented. Flexibility in the CSNS design is exploited to successfully implement the correlated painting, despite a mechanical design based on the anticorrelated painting. In Sec. III, the effectiveness of the correlated painting method is checked in both simulation and beam commissioning. The difference between the correlated and anticorrelated painting is compared in detail. By using the correlated painting method, the problems previously existed in the higher power beam commissioning are successfully solved. The summary and brief discussion are given in the last section.

II. PERFORMANCE OF THE CORRELATED PAINTING BASED ON THE MECHANICAL STRUCTURE OF THE ANTICORRELATED PAINTING SCHEME

After in-depth analysis and calculations, there are two reasons for the problems (too large beam size after painting, nonuniform beam distribution, strong transverse coupling effect, and so on) encountered in the higher power beam commissioning. First, due to an error in the mechanical design of the magnet BH3, the magnet gap can be no longer suitable for the vacuum chamber of the design size. Compared to the case of the design scheme, the actual vertical painting acceptance of the ceramic vacuum chamber at the painting magnet BH3 is much smaller, which is only about 70% of the design value (110 π mm mrad). The reduction in vertical painting acceptance leads to a significant reduction in the vertical painting range and nonuniform painting beam distribution. Second, when the beam power on the target exceeds 50 kW, the design machine mode with the nominal betatron tunes of (4.86, 4.78) will cause large coherent oscillation which produces a large amount of beam loss. To reduce the effect of coherent oscillation, new betatron tunes (4.81, 4.87) have been used to replace the nominal betatron tunes (4.86, 4.78). However, with the new betatron tunes (4.81, 4.87), the transverse coupling effect on the beam distribution is strong [27].

In order to solve the problems encountered in the higher power beam commissioning, the painting method was tried to modify when the hardware devices (vacuum chamber, injection point, etc.) and betatron tunes cannot be further optimized. A comparative study between the anticorrelated and correlated painting in the simulation shows that, for the vertical painting acceptance of about 75 π mm mrad in the injection process, the correlated painting has more advantages than the anticorrelated painting design scheme. In addition, referring to the theoretical and machine study of J-PARC on the choice of the painting method [12], because of the effect of the space-charge coupling caused by the Montague resonance, when the betatron tunes are selected close to the coupling, the anticorrelated painting has more advantages for a large painting area and the correlated painting has more advantages for a small painting area. For instance, when a painting area is about 50 π mm mrad, compared to the anticorrelated painting, the beam distribution after the correlated painting is more uniform which leads to slower emittance growth. Therefore, for the betatron tunes (4.81, 4.87) and maximum vertical painting area of about 75 π mm mrad in the CSNS/RCS, the correlated painting may have more advantages than the anticorrelated painting design scheme.

For the actual parameters of the CSNS injection system, in order to compare the correlated and anticorrelated painting in the same injection mechanical structure, the basic idea of the painting injection in terms of the painting area in comparison with the machine aperture along the injection bump orbit should be described. Then, the relationship between the emittance of the circulating beam relative to the vacuum chamber center and the machine aperture of the vacuum chamber in different painting processes needs to be figured out.

The horizontal and vertical beam sizes of the circulating beam at the injection point can be calculated by

$$\sigma_x^2 = \beta_x \varepsilon_x + D_x^2 \left(\frac{\sigma_E}{E_0}\right)^2, \tag{1}$$

$$\sigma_y^2 = \beta_y \varepsilon_y + D_y^2 \left(\frac{\sigma_E}{E_0}\right)^2, \tag{2}$$

where ε_x and ε_y are the horizontal and vertical emittances of the circulating beam, β_x and β_y are the betatron amplitude functions, D_x and D_y are the dispersion functions, σ_E is the deviation of the beam energy, and E_0 is the beam energy. Since the injection region locates in a dispersion-free drift section, we have

$$D_x \sim 0, \qquad D_y \sim 0. \tag{3}$$

During the injection process, the circulating beam center (x, y) varies with the horizontal and vertical painting curves. Then, in the painting process, the horizontal and vertical emittances of the circulating beam relative to the vacuum chamber center can be calculated by

$$\varepsilon_{rx} = \frac{[|x - x_0| + |\sigma_x|]^2}{\beta_x}, \tag{4}$$

$$\varepsilon_{ry} = \frac{[|y - y_0| + |\sigma_y|]^2}{\beta_y}, \tag{5}$$

in which (x_0, y_0) denotes the deviation position of the vacuum chamber center relative to the circulating beam after the injection. Supposing the machine aperture radius of the circular vacuum chamber be R. Then, the ratios (κ_x, κ_y) between the transverse emittances of the circulating beam relative to the vacuum chamber center and the vacuum chamber acceptances can be calculated by

$$\kappa_x = \frac{[|x - x_0| + |\sigma_x|]^2}{R^2 - (y - y_0)^2}, \tag{6}$$

$$\kappa_y = \frac{[|y - y_0| + |\sigma_y|]^2}{R^2 - (x - x_0)^2}. \tag{7}$$

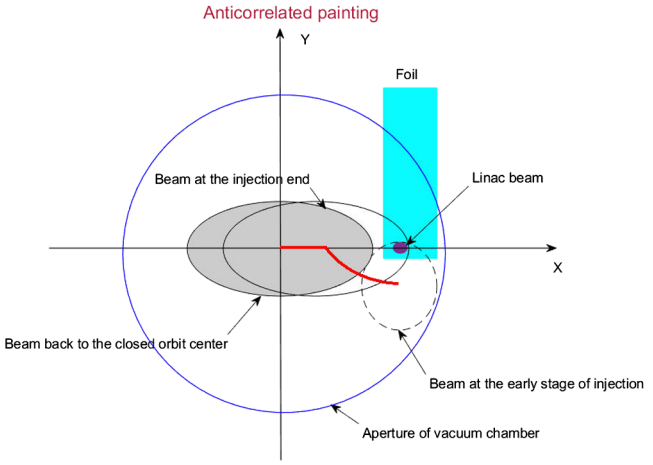

FIG. 2. Schematic drawing of the position variation of the circulating beam emittance ellipse in the anticorrelated painting process.

For the painting beam, it is necessary to focus on the ratio (κ_{xy}) between the sum of the horizontal and vertical emittances of the circulating beam relative to the vacuum chamber center and the vacuum chamber acceptance which can be calculated by

$$\kappa_{xy} = \frac{[|x - x_0| + |\sigma_x|]^2 + [|y - y_0| + |\sigma_y|]^2}{R^2}. \tag{8}$$

Therefore, the low beam loss requires that the circulating beam should meet the following conditions for each turn in the injection process:

$$\kappa_x < 1, \qquad \kappa_y < 1, \qquad \kappa_{xy} < 1. \tag{9}$$

During the anticorrelated painting process, the circulating beam moves from the positive maximum to the center in the horizontal plane and from the negative maximum to the center in the vertical plane. The injection point of the Linac beam sets at $(x_{\max}, 0)$. After the injection, the circulating beam moves rapidly to zero in both horizontal and vertical planes. Figure 2 shows the position variation of the circulating beam emittance ellipse in the anticorrelated painting process. It can be seen that, in the initial stage of the anticorrelated painting process, the vertical emittance of the circulating beam is large and the location of the vacuum chamber aperture limitation is at the bottom right corner. Therefore, the condition $\kappa_{xy} < 1$ is the main constraint for the painting beam. With the code PyORBIT [28–30], the simulation of the anticorrelated painting was done, as shown in Fig. 3. It can be seen that, for the anticorrelated painting, in the initial stage of the injection, the painting beam is easily lost at the bottom-right corner of the ceramic vacuum chamber of the magnet BH3. Therefore, in order to reduce the ratio κ_{xy}, the horizontal or vertical painting needs to be optimized. Since the position of the injection

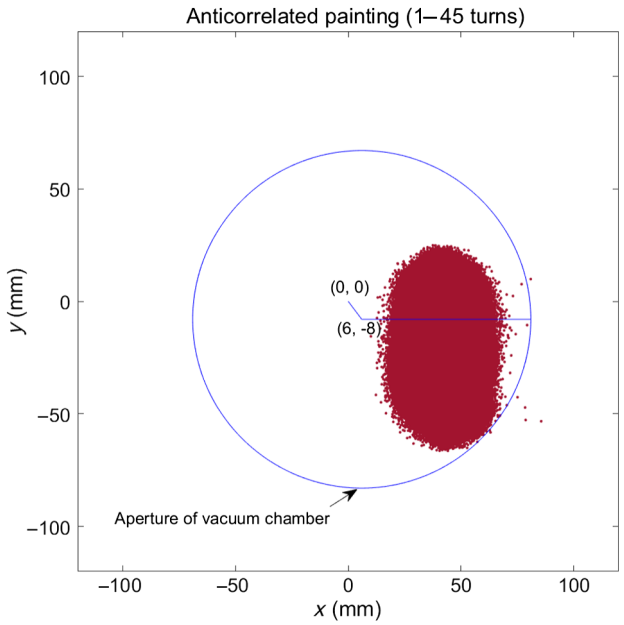

FIG. 3. Simulation results of the circulating beam distribution at the magnet BH3 in the initial stage of injection for the anticorrelated painting.

point is fixed, the circulating beam can only keep moving from the positive maximum to the center in the horizontal plane. In the vertical plane, if the circulating beam moves from the center to the negative maximum, the vertical emittance in the initial stage of the injection can be reduced, and this is the correlated painting.

For normal position scanning, the falling current curve of the pulse power supply is used to control the painting beam distribution. Based on the mechanical structure of the anticorrelated painting scheme, due to the fixed location

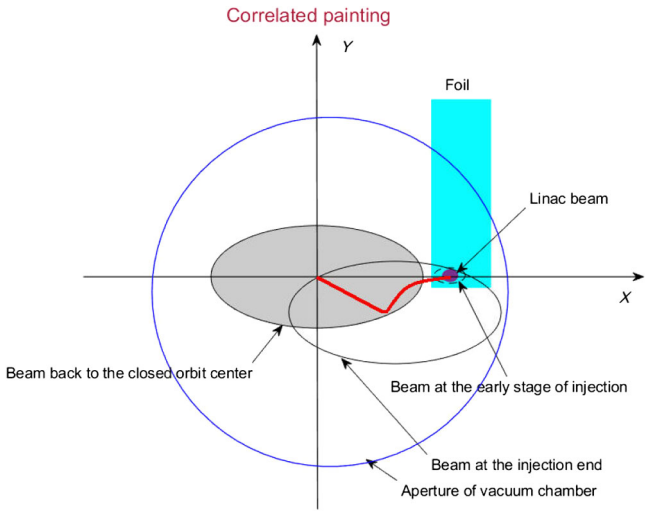

FIG. 4. Schematic drawing of the position variation of the circulating beam emittance ellipse in the correlated painting process.

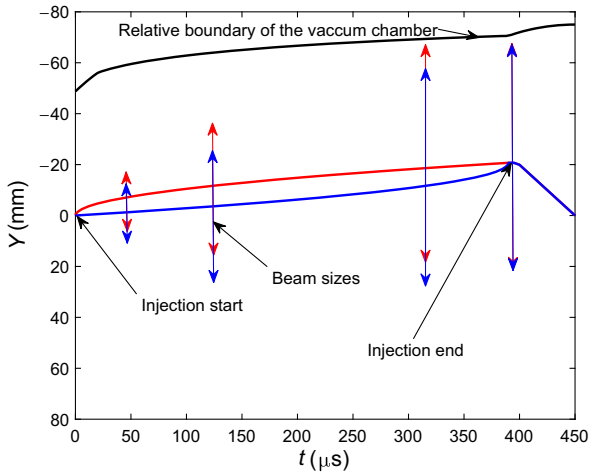

FIG. 5. Distance changing between the circulating beam and vacuum chamber for different vertical painting curves. Since the vertical painting bump is in the negative direction, the pulse current and bump position differ by a negative sign. Therefore, the Y-axis is rotated 180° to avoid misunderstanding.

of the injection point and aperture limitation of the magnets and vacuum chambers, only anticorrelated painting can be achieved by controlling the falling current curve. However, in order to achieve the correlated painting which can perform the circulating beam move from the center to the negative maximum in the vertical plane, the vertical painting by using the rising curve of the BV pulse current is proposed. During the correlated painting process, the circulating beam moves from the maximum to the center in the horizontal plane and from zero to the negative maximum in the vertical plane. After the injection, the circulating beam returns to the center orbit in both horizontal and vertical planes quickly. Figure 4 shows the position variation of the circulating beam emittance ellipse in the correlated painting process.

During the correlated painting, since the circulating beam is painted from the center to the border in the vertical

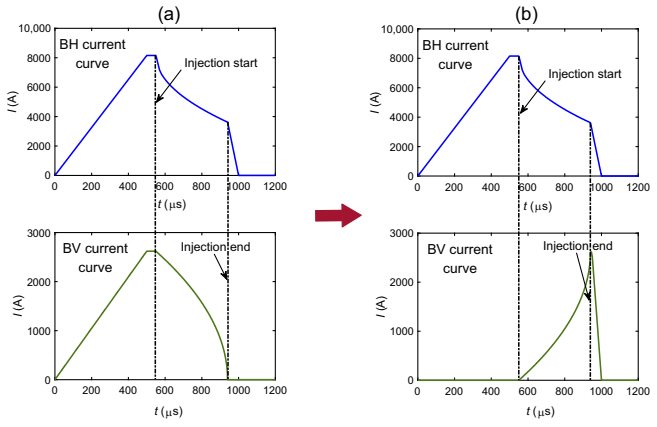

FIG. 6. BH and BV pulse current curves for the anticorrelated painting (a) and correlated painting (b).

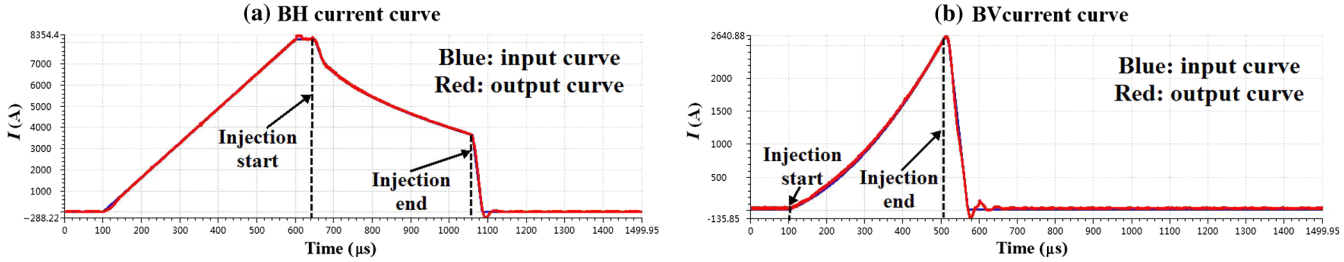

FIG. 7. Comparison of the input and output pulse current curves for the correlated painting method.

plane, the vertical size of the circulating beam increases during the injection process, as shown in Fig. 5. In the later stage of the painting, the vertical size of the circulating beam increases and the vertical painting bump is getting close to the edge of the vacuum chamber. If the painting speed on the edge is too slow, the edge particles of the circulating beam in the vertical plane may bump into the wall of the vacuum chamber which can cause beam loss. The CSNS beam commissioning results also confirm the above explanation. Therefore, the vertical painting curve has a slow painting speed in the center and a high painting speed in the border. Meanwhile, it can be seen from Fig. 5 that, with the increase of the vertical size of the circulating beam, the flattop time of the BV pulse current curve needs to be small enough. Figure 6 shows the BH and BV pulse current curves for the anticorrelated and correlated painting, respectively.

For the usage of the rising curve of the BV pulse current for the vertical painting, the rising speed, falling speed, minimum flattop time, and tracking accuracy of the BV pulse current are key issues. The experimental testing results show that the rising speed, falling speed, and tracking accuracy of the BV pulse current can meet the requirements of the correlated painting scheme. The minimum flattop time of the BV pulse current curve can reach 5 μs. Figure 7 shows the comparison of the input and output pulse current curves for the correlated painting method. It can be found that the error between the output and input pulse current curves is relatively small. Therefore, the rising part of the BV pulse current curve can be used for vertical painting.

During the correlated painting, as the preliminary design painting curves, the horizontal and vertical offsets of the time-varying closed orbit from a reference point corresponding to the unbumped closed orbit can be expressed as

$$x = x_{\max} - (x_{\max} - x_{\min})\sqrt{\frac{t}{T_{\mathrm{inj}}}}, \qquad x' = 0, \quad (10)$$

$$y = -y_{\max}\left[1 - \sqrt{1 - \frac{t}{T_{\mathrm{inj}}}}\right], \qquad y' = 0, \quad (11)$$

where $x_{\max} - x_{\min}$ is the horizontal painting range, $y_{\max}$ is the vertical painting range, and T_{inj} is the injection time. Since the injection point of the Linac beam sets at $(x_{\max}, 0)$, the maximum horizontal painting area depends on $|x_{\max} - x_{\min}|$ and the maximum vertical painting area depends on $|y_{\max}|$. In the simulation and beam commissioning, the painting curves with the square root function would be further optimized according to the results of beam injection (beam loss, beam distribution after painting, etc.).

III. SIMULATION AND BEAM COMMISSIONING OF THE CORRELATED PAINTING METHOD

The simulation is performed by using the code PyORBIT [28–30]. The injection of the correlated painting and anticorrelated painting is compared in both simulation and beam commissioning. Table II shows the injection-related parameters for the CSNS/RCS.

A. Simulation study

In the simulation, the space-charge effects are taken into account in detail [7–9]. Figure 8 shows the comparison of the transverse beam distributions for the correlated and anticorrelated painting under the same conditions. It can be found that, compared to the case of anticorrelated painting, the transverse beam size for the correlated painting is smaller and the beam distribution is much better. Figure 9 shows the comparison of the beam loss during the 200 turns injection and 2000 turns acceleration processes for different painting methods

TABLE II. Injection-related parameters for the CSNS/RCS.

Parameters (units)	Values
Injection beam energy (MeV)	80
Particle number (10^{13})	1.56
Injection time (μs)	390
Betatron tunes (ν_x, ν_y)	(4.81, 4.87)
β_x at the injection point (m)	6.4
β_y at the injection point (m)	5.7
Injection beam size (1σ) (mm)	1.0
Ring period during the injection (μs)	2.0
$x_{\max}$ (mm)	57
$x_{\min}$ (mm)	25
$y_{\max}$ (mm)	20.7

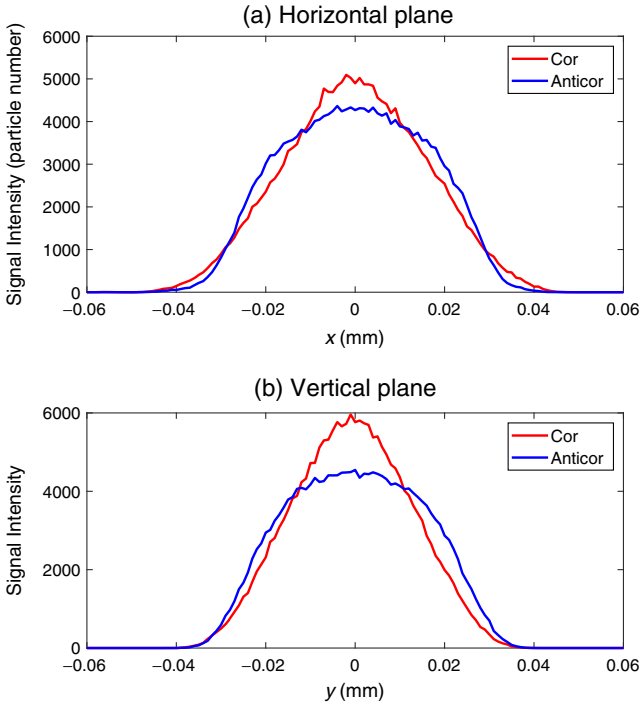

FIG. 8. Comparison of the transverse beam distributions for the correlated and anticorrelated painting in the simulation under the same conditions. Subgraph (a): horizontal beam distributions; subgraph (b): vertical beam distributions.

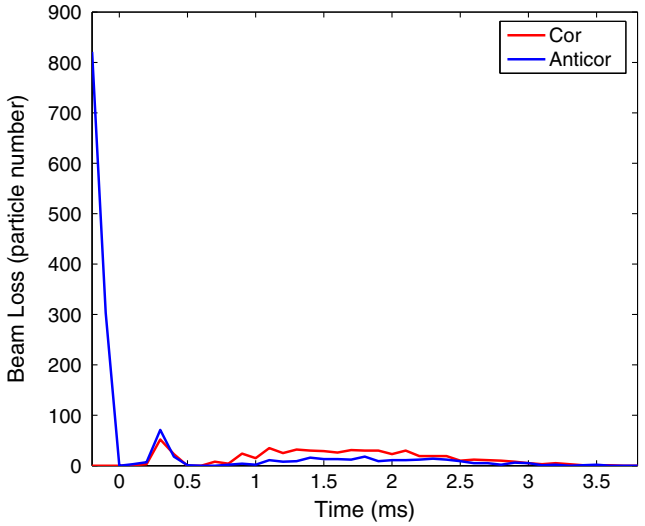

FIG. 9. Comparison of the beam loss during the 200 turns injection and 2000 turns acceleration processes for the two painting methods in the simulation under the same conditions.

under the same conditions. It can be seen that, compared to the case of anticorrelated painting, the injection beam loss for the correlated painting is reduced. Figure 10 shows the comparison of the transverse coupling effects for the two painting methods. As can be seen from the figure, for the anticorrelated painting, the variation of the vertical painting range causes observable changes in the horizontal painting distribution due to the transverse coupling effect. These changes can be reduced by using the correlated painting scheme.

The simulation results show that by using the correlated painting method, the transverse beam size is smaller, the beam distribution is much better, the injection beam loss is largely reduced, and the transverse coupling effect is dampened. In addition, the simulation results also confirm that, with the correlated painting method, the beam loss is less than 1% under the design beam power of 100 kW.

B. Beam commissioning

There are five main steps in the correlated painting commissioning: (i) the timing adjustment of the pulse power supply for the correlated painting; (ii) the parameters matching of the injection beam and circulating beam; (iii) the position adjustment of the stripping foil; (iv) the optimizations of the transverse painting ranges and painting curves; and (v) the injection beam loss control. After in-depth adjustments and optimizations, the correlated painting injection based on the mechanical structure of the anticorrelated painting scheme has been performed in the beam commissioning. In addition, a comparative study between the correlated and anticorrelated painting has been also performed.

In order to measure the transverse beam distribution after painting, a fast extraction scheme is designed by adjusting the extraction timing and extraction mode. Specifically, when the injection is completed, the circulating beam is extracted immediately and the transverse beam profile can be measured by a multiwire scanner located on the beam transport line from the RCS to the target. Furthermore, by using the beam loss monitors (BLMs) in the injection region, the injection beam loss can be observed and measured. Figure 11 shows the comparison of the transverse beam distributions for the correlated and anticorrelated painting measured in the beam commissioning. It can be seen that, compared to the case of anticorrelated painting, the transverse beam size for the correlated painting is smaller and the beam distribution is much better. The beam commissioning results are in good agreement with the simulation results shown in Fig. 8. Figure 12 shows the comparison of the injection beam loss for the correlated and anticorrelated painting, respectively, in which, all the 11 beam loss monitors are located in the injection region. The precise position of the beam loss monitor addINBLM is just at the entrance of the vacuum chamber of the magnet BH3 whose aperture is the smallest in the injection region. It can be seen that, compared to the case of anticorrelated painting, the beam loss for the correlated painting is dramatically reduced, and it is in good agreement with the simulation results shown in Fig. 9. Meanwhile, it can

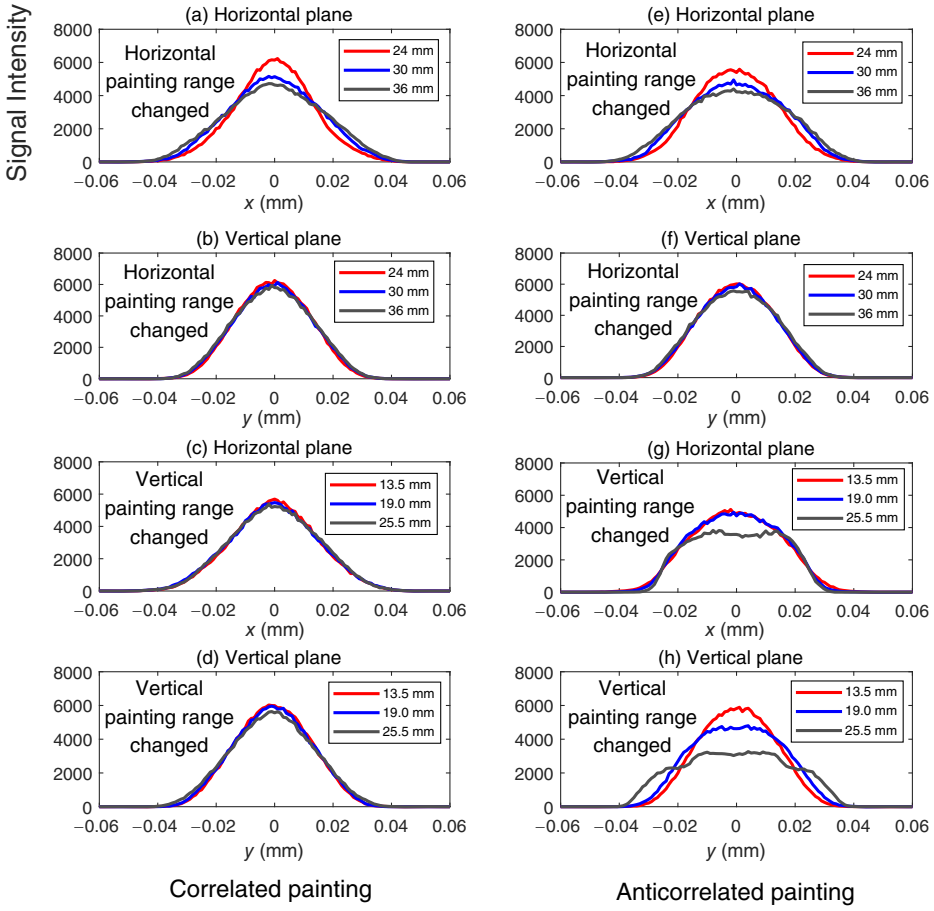

FIG. 10. Comparison of the simulation results of the transverse coupling effects for the correlated and anticorrelated painting. Subgraphs (a), (b), (e), and (f): the horizontal painting range was changed with the vertical painting range fixed to 17.5 mm; subgraphs (c), (d), (g), and (h): the vertical painting range was changed with the horizontal painting range fixed to 27 mm.

be seen from the addINBLM measurement results that, for the anticorrelated painting, the small aperture of the BH3 vacuum chamber leads to large beam loss. Figure 13 shows the comparison of the transverse coupling effects for the correlated and anticorrelated painting. It can be seen that, compared to the case of anticorrelated painting, the transverse coupling effect for the correlated painting in the vertical plane is relatively small. In addition, different from the anticorrelated painting, the correlated painting causes no significant changes in the horizontal beam distribution due to the variation of the vertical painting range. The beam

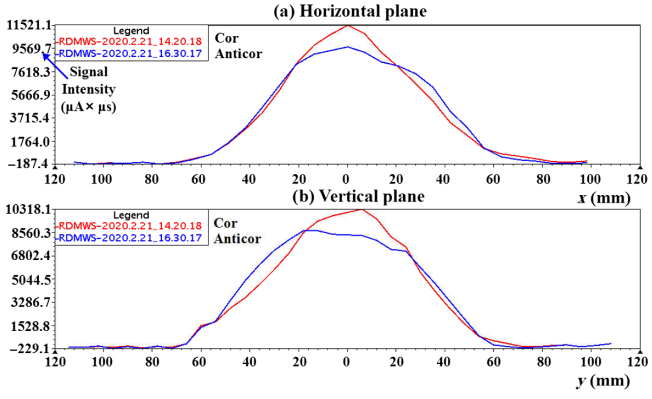

FIG. 11. Comparison of the transverse beam distributions for the correlated and anticorrelated painting in the beam commissioning. Subgraph (a): horizontal beam distributions; subgraph (b): vertical beam distributions.

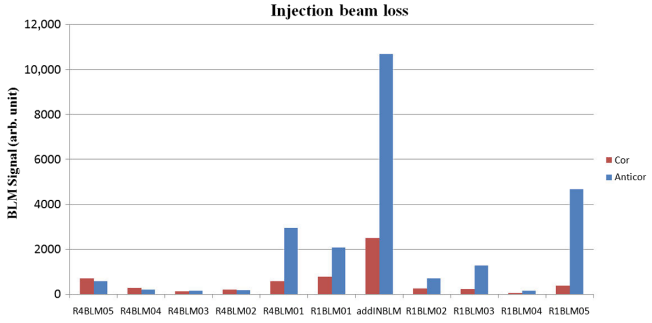

FIG. 12. The measured beam loss for the correlated and anticorrelated painting during the injection.

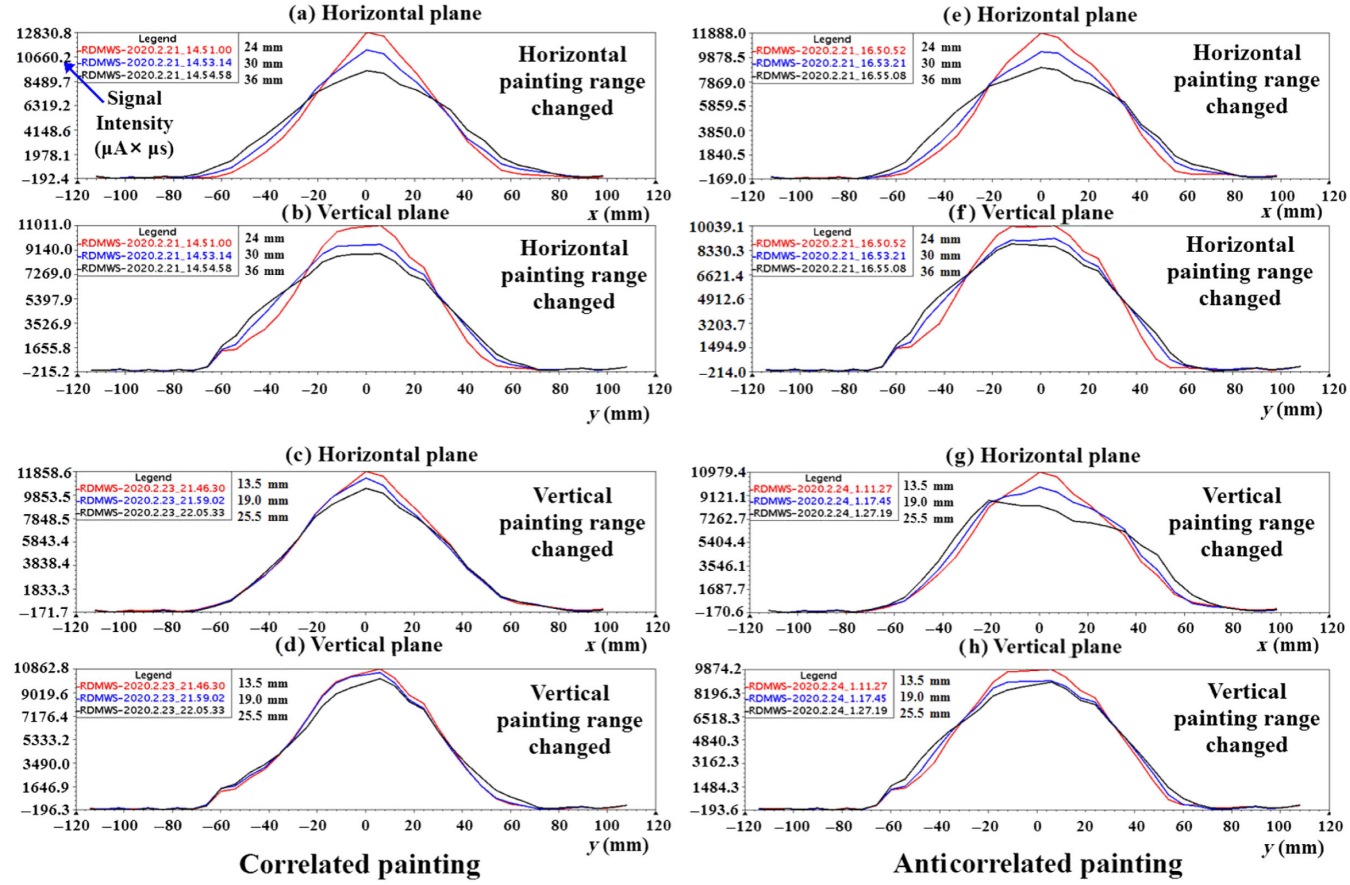

FIG. 13. The transverse coupling effects for the correlated and anticorrelated painting measured in the beam commissioning. Subgraphs (a), (b), (e), and (f): the horizontal painting range was changed with the vertical painting range fixed to 17.5 mm; subgraphs (c), (d), (g), and (h): the vertical painting range was changed with the horizontal painting range fixed to 27 mm.

commissioning results of the transverse coupling effect are somewhat different from the simulation results, but the trend is the same.

IV. SUMMARY AND DISCUSSION

Flexibility in the CSNS design was exploited to successfully implement the correlated painting, despite a mechanical design based on the anticorrelated painting. By using the code PyORBIT, the effectiveness of the correlated painting method has been investigated. The correlated painting method has been successfully applied to the beam commissioning for the CSNS/RCS. The simulation and beam commissioning results show that, compared to the case of anticorrelated painting, the transverse beam size for the correlated painting is largely reduced, the beam distribution becomes more uniform, the injection beam loss is reduced, and the transverse coupling effect is also improved. By using the new method, the problems in the higher power beam commissioning have been successfully solved. The beam power on the target has successfully risen from 50 kW to the design value of 100 kW, and the machine has been operated stably in the user mode.

Under the mechanical structure of the anticorrelated painting scheme where the position scanning is used in both horizontal and vertical planes, the correlated painting is successfully achieved by using the rising current curve. Therefore, the correlated painting and anticorrelated painting can be well switched.

ACKNOWLEDGMENTS

The authors would like to thank H. C. Liu, Y. L. Zhang, W. Q. Zhang, G. Z. Zhou, P. Zhu, Z. H. Xu, Y. S. Yuan, and other CSNS colleagues for helpful discussions. This work is jointly supported by the National Natural Science Foundation of China (Projects No. 12075134 and No. U1832210) and the Guangdong Basic and Applied Basic Research Foundation (Project No. 2021B1515120021).

[1] J. Wei, H. S. Chen, Y. W. Chen *et al.*, China Spallation Neutron Source: Design, R&D, and outlook, Nucl. Instrum. Methods Phys. Res., Sect. A **600**, 10 (2009).

[2] J. Wei, Synchrotrons and accumulators for high-intensity proton beams, Rev. Mod. Phys. **75**, 1383 (2003).

[3] S. Wang, S. X. Fang, S. N. Fu, W. B. Liu, H. F. OuYang, Q. Qin, J. Y. Tang, and J. Wei, Introduction to the overall physics design of CSNS accelerators, Chin. Phys. C **33**, 1 (2009).

[4] J. Wei, S. N. Fu, J. Y. Tang, J. Z. Tao, D. S. Wang, F. W. Wang, and S. Wang, China Spallation Neutron Source—an overview of application prospects, Chin. Phys. C **33**, 1033 (2009).

[5] M. Y. Huang, S. Wang, J. Qiu, N. Wang, and S. Y. Xu, Effects of injection beam parameters and foil scattering for CSNS/RCS, Chin. Phys. C **37**, 067001 (2013).

[6] X. H. Lu, M. Y. Huang, and S. Wang, Injection orbit matching for a rapid cycling synchrotron, Phys. Rev. Accel. Beams **21**, 062802 (2018).

[7] J. A. Holmes, V. V. Danilov, J. D. Galambos, D. Jeon, and D. K. Olsen, Space charge dynamics in high intensity rings, Phys. Rev. ST Accel. Beams **2**, 114202 (1999).

[8] S. Cousineau, S. Y. Lee, J. A. Holmes, V. Danilov, and A. Fedotov, Space charge induced resonance excitation in high intensity rings, Phys. Rev. ST Accel. Beams **6**, 034205 (2003).

[9] S. Y. Xu and S. Wang, Study on space charge effects of the CSNS/RCS, Chin. Phys. C **35**, 1152 (2011).

[10] J. Wei, J. Beebe-Wang, M. Blaskiewicz *et al.*, Injection choice for Spallation Neutron Source Ring, in *Proceedings of the 2001 Particle Accelerator Conference, Chicago, IL, 2001* (IEEE, Piscataway, NJ, 2001), pp. 2560–2562.

[11] J. Beebe-Wang, Y. Y. Lee, D. Raparia, and J. Wei, Transverse phase space painting for SNS accumulator ring injection, in *Proceedings of the 18th Particle Accelerator Conference, New York, 1999* (IEEE, New York, 1999), pp. 1743–1745.

[12] H. Hotchi, Effects of the Montague resonance on the formation of the beam distribution during multiturn injection painting in a high-intensity proton ring, Phys. Rev. Accel. Beams **23**, 050401 (2020).

[13] H. Hotchi, High-power proton accelerators for pulsed spallation neutron sources, AAPPS Bull. **31**, 23 (2021).

[14] Spallation Neutron Source: Description of accelerator and target, edited by B. Boardman, Rutherford Appleton Laboratory Report No. RL-82-006, 1982.

[15] D. J. S. Findlay, D. J. Adams, T. A. Broome *et al.*, ISIS Upgrades-A Status Report, in *Proceedings of the 10th European Particle Accelerator Conference, Edinburgh, Scotland, 2006* (EPS-AG, Edinburgh, Scotland, 2006), pp. 935–939.

[16] J. D. Galambos, J. A. Holmes, Y. Y. Lee, A. Luccio, D. K. Olsen, and J. Beebe-Wang, Status of the SNS injection system, in *Proceedings of the 6th European Particle Accelerator Conference, Stockholm, Sweden, 1998* (EPS-AG, Stockholm, Sweden, 1998), pp. 341–343.

[17] S. Henderson, W. Abraham, A. Aleksandrov *et al.*, The Spallation Neutron Source accelerator system design, Nucl. Instrum. Methods Phys. Res., Sect. A **763**, 610 (2014).

[18] J. Y. Tang, J. Qiu, S. Wang, and J. Wei, Physics design and study of the BSNS RCS injection system, Chin. Phys. C (HEP & NP) **30**, 1184 (2006), http://hepnp.ihep.ac.cn/article/id/61bf5506-ad75-47fd-8296-0ee80a0e8e1c.

[19] High-Intensity Proton Accelerator Project Team, Accelerator technical design report for high-intensity proton accelerator facility project, JAERI Report No. JAERI-Tech2003-044, 2003.

[20] I. Sakai, Y. Arakida, I. Sugai *et al.*, H^- painting injection system for the J-PARC 3-GeV high intensity proton synchrotron, in *Proceedings of the 8th European Particle Accelerator Conference, Paris, France, 2002* (EPS-AG, Paris, France, 2002), pp. 1040–1042.

[21] F. Naito, J-PARC accelerator status, Nucl. Part. Phys. Proc. **273–275**, 181 (2016).

[22] P. K. Saha, Y. Shobuda, H. Hotchi, N. Hayashi, T. Takayanagi, H. Harada, and Y. Irie, Direct observation of the phase space footprint of a painting injection in the Rapid Cycling Synchrotron at the Japan Proton Accelerator Research Complex, Phys. Rev. ST Accel. Beams **12**, 040403 (2009).

[23] H. Hotchi, H. Harada, N. Hayashi *et al.*, Beam loss reduction by injection painting in the 3-GeV rapid cycling synchrotron of the Japan Proton Accelerator Research Complex, Phys. Rev. ST Accel. Beams **15**, 040402 (2012).

[24] P. K. Saha, H. Harada, N. Hayashi *et al.*, Beam emittance control by changing injection painting area in a pulse-to-pulse mode in the 3-GeV rapid cycling synchrotron of Japan Proton Accelerator Research Complex, Phys. Rev. ST Accel. Beams **16**, 120102 (2013).

[25] H. Hotchi, N. Tani, and Y. Watanabe, Numerical study for beam loss occurring for wide-ranging transverse injection painting and its mitigation scenario in the J-PARC 3-GeV RCS, Nucl. Instrum. Methods Phys. Res., Sect. A **778**, 102 (2015).

[26] H. Hotchi, N. Tani, Y. Watanabe, H. Harada, S. Kato, K. Okabe, P. K. Saha, F. Tamura, and M. Yoshimoto, Beam loss caused by edge focusing of injection bump magnets and its mitigation in the 3-GeV rapid cycling synchrotron of the Japan Proton Accelerator Research Complex, Phys. Rev. Accel. Beams **19**, 010401 (2016).

[27] M. Y. Huang, S. Y. Xu, Y. W. An *et al.*, Study on the anti-correlated painting injection scheme for the Rapid Cycling Synchrotron of the China Spallation Neutron Source, Nucl. Instrum. Methods Phys. Res., Sect. A **1007**, 165408 (2021).

[28] J. Gabambos, S. Danilov, D. Jeon, J. Holmes, D. Olsen, J. Beebe-Wang, and A. Luccio, ORBIT—a ring injection code with space charge, in *Proceedings of the 18th Particle Accelerator Conference, New York, 1999* (IEEE, New York, 1999), pp. 3143–3145.

[29] J. F. Ostiguy and J. Holmes, PyORBIT: A Python shell for ORBIT, in *Proceedings of the 2003 Particle Accelerator Conference, Portland, OR, 2003* (IEEE, New York, 2003), pp. 3503–3505.

[30] A. Shishlo, S. Cousineau, J. Holmes, and T. Gorlov, The particle accelerator simulation code PyORBIT, Procedia Comput. Sci. **51**, 1272 (2015).